

2

**AD-A230 998**

**DTIC FILE COPY**  
**MODELING FAILURE AND RELIABILITY**  
**IN NEW-GENERATION DEVICES**

**FINAL REPORT**

Jeffrey Frey

July 15, 1990

Grant Number DAAL03-88-K-0115

University of Maryland  
College Park, MD 20742

**DTIC**  
**ELECTE**  
**JAN 15 1991**  
**S B D**

Approved for Public Release  
Distribution Unlimited

REPORT DOCUMENTATION PAGE

REPORT SECURITY CLASSIFICATION <u>Unclassified</u>		1b. RESTRICTIVE MARKINGS	
SECURITY CLASSIFICATION AUTHORITY		3. DISTRIBUTION / AVAILABILITY OF REPORT Approved for public release; distribution unlimited.	
DECLASSIFICATION / DOWNGRADING SCHEDULE		5. MONITORING ORGANIZATION REPORT NUMBER(S) <u>ARO 25842.5-EL</u>	
PERFORMING ORGANIZATION REPORT NUMBER(S)		7a. NAME OF MONITORING ORGANIZATION U. S. Army Research Office	
NAME OF PERFORMING ORGANIZATION University of Maryland	6b. OFFICE SYMBOL (If applicable) N/A	7b. ADDRESS (City, State, and ZIP Code) P. O. Box 12211 Research Triangle Park, NC 27709-2211	
ADDRESS (City, State, and ZIP Code) College Park, MD 20742		9. PROCUREMENT INSTRUMENT IDENTIFICATION NUMBER <u>DAAL03-88-K-0115</u>	
NAME OF FUNDING / SPONSORING ORGANIZATION U. S. Army Research Office	6b. OFFICE SYMBOL (If applicable)	10. SOURCE OF FUNDING NUMBERS	
ADDRESS (City, State, and ZIP Code) P. O. Box 12211 Research Triangle Park, NC 27709-2211		PROGRAM ELEMENT NO.	PROJECT NO.
		TASK NO.	WORK UNIT ACCESSION NO.
TITLE (Include Security Classification) Modeling Failure and Reliability in New-Generation Devices - Final Report (Unclassified)			
PERSONAL AUTHOR(S) Jeffrey Frey			
TYPE OF REPORT Final	13b. TIME COVERED FROM 1988 TO 1990	14. DATE OF REPORT (Year, Month, Day) 90-7-15	15. PAGE COUNT 0
SUPPLEMENTARY NOTATION The view, opinions and/or findings contained in this report are those of the author(s) and should not be construed as an official Department of the Army position, policy, or decision, unless so designated by other documentation.			
COSATI CODES		18. SUBJECT TERMS (Continue on reverse if necessary and identify by block number)	
FIELD	GROUP	SUB-GROUP	
		Semiconductor Devices; reliability; hot electrons; gallium Arsenide; MESFETS; Energy Transport; impact ionization.	
ABSTRACT (Continue on reverse if necessary and identify by block number)			
<p>A two-dimensional device simulation program (JUMDFET) designed to produce information on the reliability of both silicon and compound-semiconductor electron devices was constructed. The program uses either the drift-diffusion description of carrier transport, for relatively large devices, or the newer energy transport method of solving the Boltzmann Transport Equation, for submicron-scale devices. Multi-layered heterostructure MESFETs, as well as silicon MOSFETs, may be simulated. UJUMDFET has been used to examine performance and reliability of silicon MOSFETs with channel lengths below 0.2 micron, showing that reliability of such small devices is not as great a problem as was originally thought.</p> <p>This report comprises abstracts of papers submitted, presented at conferences, and published in journals, based on work performed under the referenced grant.</p>			
DISTRIBUTION / AVAILABILITY OF ABSTRACT UNCLASSIFIED UNLIMITED <input type="checkbox"/> SAME AS RPT. <input type="checkbox"/> DTIC USERS		21. ABSTRACT SECURITY CLASSIFICATION Unclassified	
NAME OF RESPONSIBLE INDIVIDUAL		22b. TELEPHONE (Include Area Code)	22c. OFFICE SYMBOL

**MODELING FAILURE AND RELIABILITY**

**IN NEW-GENERATION DEVICES**

**Grant Number DAAL03-88-K-0115**

**FINAL REPORT - July, 1990**

**Jeffrey Frey  
University of Maryland  
College Park, MD 20742**

1. **UMDFET - A Two-Dimensional General Device Simulator and its Application in EPROM Analysis**  
M.S. thesis, Z.Z.Peng (*Abstract*)
2. **UMDFET2.0 - A Two-Dimensional General Device Simulator, User's Manual.** (*Section 1.1 - general information*)
3. **Device Simulation for 0.1 micron MOSFETs - Performance and Reliability.** (*Abstract of paper presented at VLSI Device and Process Simulation Workshop, Osaka, Japan, May, 1989*)
4. **Susceptibility of Gallium Arsenide Amplifiers to Single Pulses of Intense Microwave Radiation.** (*Paper presented at GOMAC-90 Conference, Las Vegas, NV, November, 1990*)
5. **Rectification Failure in GaAs MESFETs Subjected to Single Pulses of Intense Microwave Radiation.** (*Abstract of Paper presented at 1990 IEEE Microwave and Millimeter-Wave Integrated Circuits Conference, May, 1990*)
6. **Enhanced Reliability in Si MOSFET's With Channel Lengths Under 0.2 Micron.** (*Extended abstract of paper published in Solid-State Electronics 33, 1275 (1990)*)
7. **Efficient Calculation of Ionization Coefficients in Silicon from the Energy Distribution Function**  
(*Abstract of paper published in J. Appl. Physics 68, 1075 (1990)*)
8. **RELY: A Physics-Based CAD Tool for Time-Dependent Hot-Electron Induced MOSFET Reliability Investigations**  
(*Paper presented at 1990 International Devices and Materials Conference, Taipei, Taiwan, November, 1990*)
9. **Mosfet Hot-Electron gate Current Calculation by Combining Energy Transport Method with Monte Carlo Simulation**  
(*Paper to be presented at 1990 International Electron Devices Meeting, San Francisco, December, 1990*)

## ABSTRACT

Title of Thesis:

### UMDFET — A TWO-DIMENSIONAL GENERAL DEVICE SIMULATOR AND ITS APPLICATION IN EPROM ANALYSIS

Name of degree candidate: Zezhong Peng

Degree and Year: Master of Science 1989

Thesis directed by: Jeffrey Frey, Professor of Electrical Engineering Department

A generalized single-electron-gas energy transport model for simulation of sub-micrometer dimension GaAs devices is described, in which the effects of the heat flux and the potential energy of the electrons in the upper valley are included. The electron temperature includes the effect of introduction of the potential energy. A numerical method for rigorous solution of the current continuity and energy transport equations is presented. A two-dimensional general device simulator — UMDFET was developed using some of the principles of the model and has been used to simulate EPROM devices.

<b>Accession For</b>	
NTIS GRA&I	<input checked="" type="checkbox"/>
DTIC TAB	<input type="checkbox"/>
Unannounced	<input type="checkbox"/>
Justification	
By _____	
Distribution/	
<b>Availability Codes</b>	
Dist	Avail and/or Special
A-1	

# **UMDFET2.0**

**A TWO-DIMENSIONAL  
GENERAL DEVICE SIMULATOR**

**USER'S MANUAL**

**Zezhong Peng**

**Jeffrey Frey**

**Electrical Engineering Department**

**The University of Maryland**

**U.S.A.**

**August, 1990**

# Chapter 1

## General Information

**UMDFET** (University of Maryland **F**ield-**E**ffect **T**ransistor Simulator) [1,2,3,4, 5,6] is an newly developed, user-oriented, two-dimensional numerical device simulation program, which may be used for MOSFETs, LDD devices, MESFETs, HEMTs and planar multi-layer structures. The device material can be Si, GaAs or any other material for which a user can provide characteristics. Both a drift-diffusion (DD) model and an energy transport (ET) model are available. In the latter, the two-dimensional energy balance equations are rigorously solved, including heat flux and diffusion terms, and impact ionization as well as the potential energy of electrons in satellite valleys in compound semiconductors. UMDFET is capable of simulating the performance and reliability of devices with deep submicron channel lengths and under high bias operation.

## 1.1 User's Guide

**UMDFET** is a friendly simulation program which can interact with a user, and guide the user to a successful simulation.

**UMDFET** has the following capabilities:

1. With the energy transport model, **UMDFET** can accurately simulate devices with effective channel lengths below 0.1 micron. Such short-channel effects as velocity overshoot and electron temperature lowering are accurately described[4,5]. Refer to TM of **OPTION** card in Chapter 2.
2. **UMDFET** is able to calculate hot electron induced gate injection current and substrate current [3,6]. Refer to IG in **OUTPUT** card for gate current; IMP and TM in **OPTION** card and IMP in **OUTPUT** card for substrate current.
3. User can easily specify materials, i.e, Si and GaAs, or any other material whose characteristics are known. Refer to **LAYER** in Chapter 2.
4. Capability of analysis of planar multi-layer device structures enables user to simulate conventional MOSFETs, LDD MOSFETs, MESFETs and HEMTs. Refer to **DEVICE**, **LAYER**, **PROFILE**, **IMPLANT** and **LDDIMP** cards in Chapter 2.
5. User can get on-line information on the **UMDFET** simulation process by specifying **PRINTLEVEL**, so he/she can check whether the simulation is processing properly.
6. Convergence at very high bias is good. Methods of global convergence checking, 2D potential extrapolation and convergence refining are used to improve convergence[2,3]. Refer to **OPTION** and **END** cards in Chapter 2.

7. User has good control of **UMDFET** in order to achieve optimum simulation on a specific problem. Refer to **INTBIN**, **NREFINE**, **MCYCLE**, **ERROR** and **PRINT** in Chapter 2.
8. **UMDFET** has two kinds of simulation bias modes, i.e., an I-V curve generating bias mode and an EPROM bias mode. Refer to **BIAS** and **STEP**.
9. **UMDFET** can use previous **UMDFET** simulation results as an initial guess for a new simulation. User can refine the convergence of a previous simulation to any desired level, so that a hard-convergence problem can be solved incrementally. Refer to **INTBIN** and **NREFINE** in **OPTION** in Chapter 2.
10. User has three options for mesh generation:
  - 1) user defined mesh;
  - 2) taking a mesh from **UMDFET.INT**;
  - 3) auto-mesh generation.Refer to **MESH** in Chapter 2.
11. Auto-mesh updating.
12. Versatile doping profile generation.  
Refer to **PROFILE** and **LDD** in Chapter 2.
13. Good interfaces. Refer to **UMDFET File System and Block Diagram**.

## DEVICE SIMULATION FOR 0.1 MICRON MOSFETS - Performance and Reliability

Jeffrey Frey

University of Maryland, College Park, MD 20742

The Energy Transport (ET) method for solution of the Boltzmann Transport Equation is an efficient and economical approach to the simulation of the performance and reliability of devices with active lengths down to only hundreds of Angstroms. This method is rapid enough, even with accuracy-enhancing measures taken, and when applied to two-dimensional problems, to be used at an individual engineer's workstation.

While original ET device simulations were confined to use of a symmetrical distribution function, current simulations using this method either add an additional moment equation, to account for heat flow, or approximate the distribution function with physically reasonable functions. We have adopted the latter approach, and incorporated the method into our two-dimensional device simulation program UMDFET. [1] The distribution function we use is an expansion in Legendre polynomials, to account for a spherically symmetrical and an asymmetrical component, and yields energy distribution function results very close to those obtained by MC simulations--at a very small fraction of the cost. In addition, use of this expansion allows the ET moment equations to be expressed in very simple and easily calculable form.

We have used these methods in our two-dimensional ET program to study n-channel silicon MOSFETs with gate lengths between 0.05 and 0.25 microns. With constant-field scaling, maximum electron temperature in these devices decreases significantly as channel length decreases, for channel lengths less than 0.18 microns. This phenomenon, which is a result of the decreased ratio of electron transit time to energy relaxation time as gate lengths are shortened, indicates that short-channel devices can be more reliable than similar long channel devices, as indicated also by recent experiments. [2]

Our short-channel ET simulations, which require only SUN-level workstations, show that hot-electron related MOSFET reliability problems should become less threatening for silicon MOSFETs with very short channel lengths. These simulations will be equally useful for predicting basic device performance factors, as well--if suitable process-related constants can be obtained--as for predicting device reliability.

---

[1] Z. Peng, "UMDFET A Two-dimensional General Device Simulator and its Application in EPROM Analysis", Master's Thesis of 1989, in the University of Maryland.

[2] G.G. Shahidi, D.A. Antoniadis, and H.I. Smith, "Reduction of Channel Hot-Electron-Generated Substrate Current in Sub-150nm Channel Length Si MOSFET", IEEE Electron Device Letters, vol. 9, no. 10, p. 497, 1988.

## SUSCEPTIBILITY OF GALLIUM ARSENIDE AMPLIFIERS TO SINGLE PULSES OF INTENSE MICROWAVE RADIATION

John H. McAdoo, W. Michael Bollen, Robert Seeley, Will Caroe  
Mission Research Corp., Newington, Va.  
Jeffrey Frey  
Department of Electrical Engineering  
University of Maryland, College Park, Md.

Gallium arsenide (GaAs) monolithic microwave integrated circuits (MMICs) are starting to be inserted into military systems because they are extremely compact, light weight, and have low power requirements. Because of their low noise figure, the smallest and most sensitive of these devices are expected to find especially wide use as receivers for radar frequency signals and herein lies a problem. The submicron transistor elements have low heat capacity and therefore it takes little energy to heat them to point of permanent damage. An aircraft employing GaAs MMIC radar receivers can expect to have the receivers damaged by a close approach to any powerful search radar. But even worse, the incorporation of these devices into our military systems will give an enemy an incentive to develop electromagnetic directed energy systems capable of destroying the small transistors from ranges of several kilometers. For many applications it will be possible to protect the receivers by placing a conventional limiting diode between the antenna and the receiver. However, for phased array radar the packing density of the individual receiver elements will have to be too high to permit the inclusion of macroscopic power limiting diodes and therefore a microscopic solution for hardening the system must be found.

Figure 1 shows a typical experimental setup used for determining susceptibility and for studying damage mechanisms. The circuit is used to measure the power input to the device under test (DUT), the output power and the power reflected in the fundamental frequency and several harmonics.

Microwave radiation from a directed energy weapon is expected to consist of a single intense microwave pulse lasting from 10 to 100 ns at 1 to 12 GHz with an intensity on target as high as 1 Kw/cm<sup>2</sup>. In the laboratory, we have simulated this environment by injecting single pulses of radiation into the input ports of unprotected devices. The testing procedure to determine susceptibility was similar for all devices. First a low-power pulse was used to verify that the device was functioning normally. Successive pulses were then applied with 6dB power increments until the device was damaged. Damage was ascertained through various techniques. In the early tests, the bias currents, noise figure and small signal gain were measured after each pulse. A change in noise figure of 1/2 dB was a significant indicator of damage and was always accompanied by a correspondingly significant reduction in small signal gain. As the testing proceeded, it became apparent that visual inspection of the circuit at a magnifi-

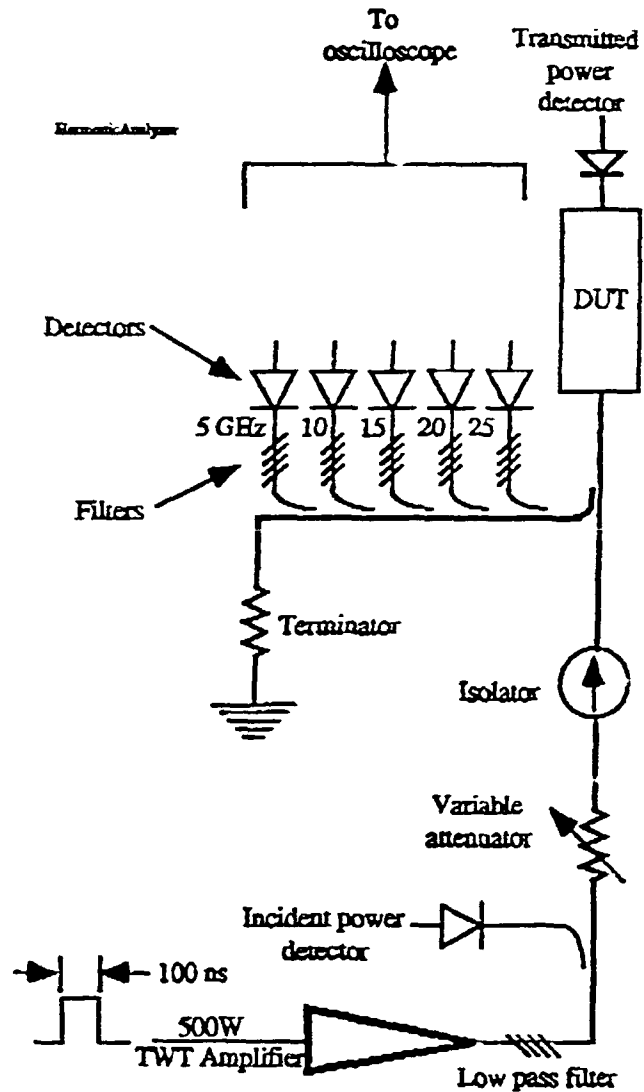


Figure 1

A typical experimental setup for susceptibility tests and hardening related studies.

cation of about 500X often provided an even more stringent test for damage than either noise figure or small signal gain, and therefore, in the later tests, we used only visual checks and changes in small signal gain as indicators of damage.

Figure 2 exhibits the main results of our susceptibility tests. It shows the device type vs the incident energy in the pulse that resulted in detectable damage. The length of the black bars is proportional to the average of all the

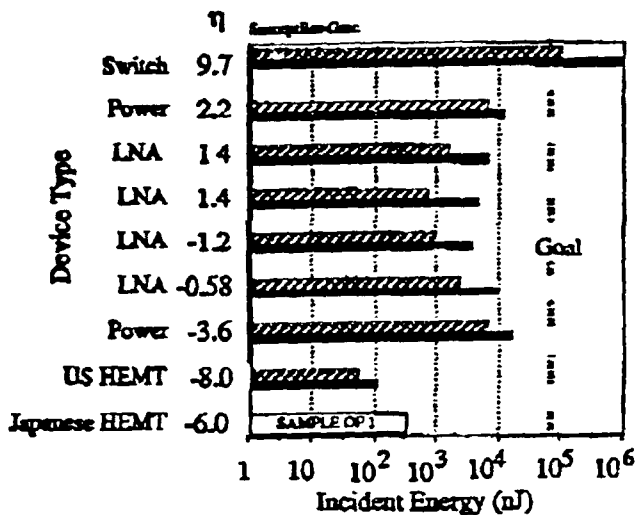


Figure 2

Incident energy for failure for various device types. If the incident energy is less than that shown by the striped bars, the device will survive, but if it is greater than the black bars, the device will certainly fail. The tests are listed in order of frequency match between the device design frequency and the test frequency. The

last shots for the corresponding device type tested, while the length of the grey bars is proportional to the average of all the penultimate shots. If one applies more incident energy than that shown by a dark bar, the device will probably fail, but if one applies less than that shown by the grey, the device will most likely survive. The device types are abbreviated as follows: Power = GaAs MESFET power amplifier, LNA = low noise amplifier employing GaAs metal-semiconductor field effect transistor (MESFET), HEMT = low noise amplifier employing high electron mobility transistors. Along the vertical axis, with the device types, is a number,  $\eta$ , that indicates the frequency match between the test frequency and the design frequency of the device,

$$\eta = 10 \log \left( \frac{f_t - f_0}{\Delta f} \right) \quad 1$$

where  $f_t$  is the test frequency,  $f_0$  the design frequency and  $\Delta f$  the bandwidth. The devices are listed in order of frequency match, with the worst match at the top. Among the low-noise amplifiers, one can discern a slight trend toward greater susceptibility as the frequency match improves. The relation is weak because the reflectivity of the in-band devices increases with increasing incident power, while that of the out-of-band devices decreases. This is a result of the power dependence of transistor impedance. One low noise amplifier bucks the trend. This employs a Japanese transistor designed with a larger number of narrower gates than its American counterparts.

Focussing on the overall picture, the tests show that GaAs MMIC and MIC devices fail at stress levels that are one order of magnitude less than the goals set by military

planners. Especially worrisome are the results on devices employing high electron mobility transistors (HEMTs). These are more susceptible by an order of magnitude than the older metal field effect transistor technology.

The susceptibility tests that indicated the problem were largely completed in 1987. Although susceptibility tests are continuing as new devices are made available, our efforts have shifted towards research aimed at hardening solutions. These solutions fall into two categories: techniques that limit the power transmitted to the sensitive-MESFET gates, and techniques that enable the gates to withstand greater abuse. We have been focusing on the

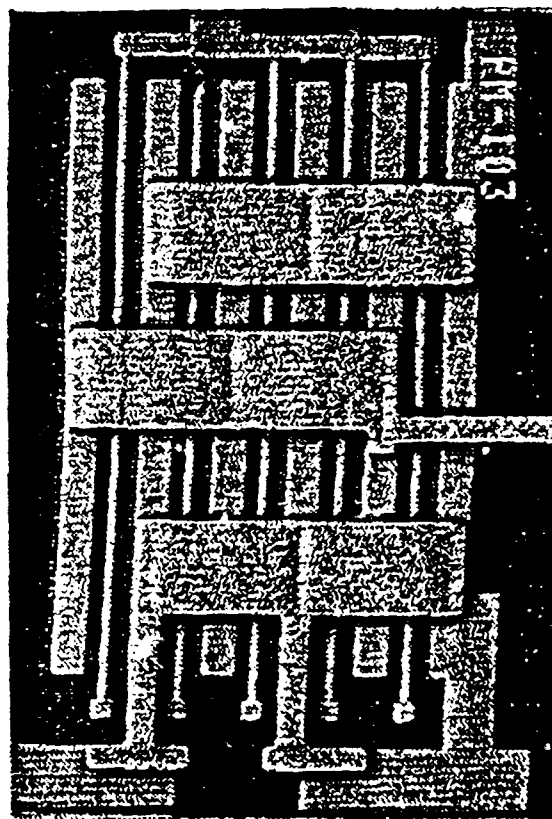


Figure 3

Damage to a MESFET gate from a 9GHz, 10ns pulse at 360W.

later category by studying damage mechanisms. Early studies using photomicrographs of damaged gates (Figure 3) revealed that the energy deposition is concentrated at gate necks. These results suggest that the corners of the source and drain electrodes should be rounded to reduce electric field concentrations and ballast resistance should be added to spread the energy more evenly over the various parallel gate channels.

More recent work employing spectroscopy and high speed photographs of developing sparks has revealed a failure mode called rectification failure common to GaAs MESFETs. The mechanism results in the destruction of the rectifying property of the Schottky junctions. A junc-

tion that has so failed can no longer block the flow of current in either direction and acts as an ordinary ohmic resistor. Catastrophic failure follows from current driven by bias voltages through the failed junction.

Previous investigators employing trains of lower power pulses had identified metal migration as a key failure mode for extended exposure to moderate levels of microwave radiation<sup>1-5</sup>. However, we have found the failure signature to be different when damage is caused by single high power microwave pulses lasting for a time short compared to the thermal transfer time of a MESFET gate<sup>6</sup>. In 1986 Anderson<sup>7</sup> described a single pulse failure mechanism called "subsurface burnout." He based his arguments on postmortem observations of the surfaces of the damaged devices.

Rectification failure differs significantly from subsurface burnout. We have identified rectification failure with a combination of diagnostic techniques never before brought to bear. High-speed photography was used to clock the emission of optical radiation after the arrival of the high power microwave pulse, optical spectroscopy was employed to determine the source of the optical emissions, and rf spectroscopy was applied to monitor the generation of harmonics of the incident radiation as a function of time during each test pulse. Devices tested included packaged low-noise amplifiers, and power amplifiers.

The high-speed photographs were obtained with an optical streak camera. Figure 4 is a superposition of the image of the circuit with the streaked image of a spark that burned at the point marked with the arrow. The figure shows that the spark first became visible about 1.25  $\mu$ s after the arrival of the microwave pulse. This is somewhat

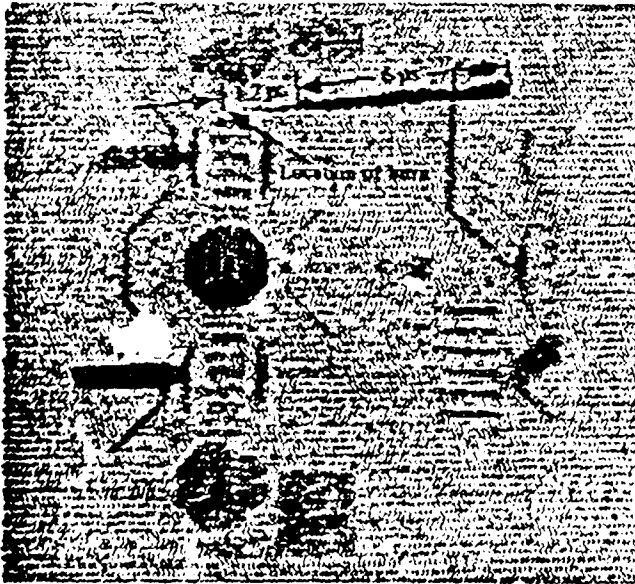


Figure 4

Streak photograph showing the time development of a spark on a MESFET. The spark lasted longer than the rf test pulse that supposedly generated the spark.

remarkable considering that the microwave pulse only lasted for 80 ns. Even more revealing is the growth in brightness of the spark for the remaining 6  $\mu$ s of the streak camera sweep period. The circuit shown in Figure 4 was a power amplifier fully biased for normal operation. Rectification failure occurred possibly through rf heating of the Schottky junction. After the rf pulse had passed, the reverse bias potentials were able to drive currents that gradually heated the gate to incandescence. This incandescence was recorded by the streak camera as a spark of growing intensity.

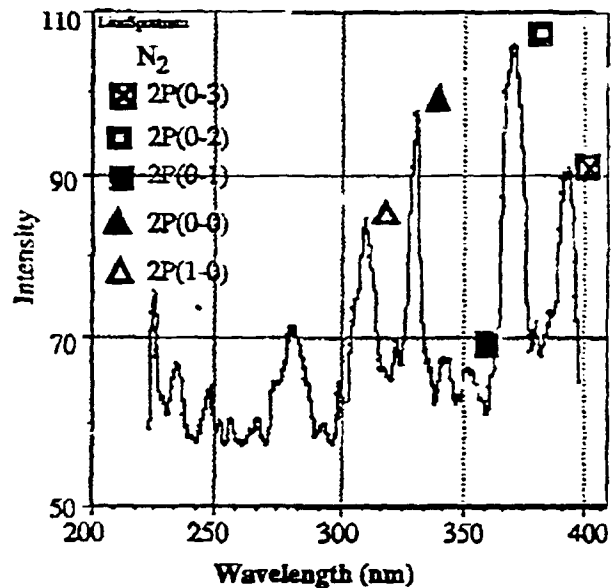


Figure 5

Nitrogen line radiation emitted by a spark from an unbiased device indicates an arc between electrodes on the surface of the MMIC.

sity.

A spectrograph of the light emitted from a similar device, likewise biased for normal operation, indicated a continuous spectrum over the range of the field of view ( $432 < \text{wavelength } (\lambda) < 632$  nanometers). Figure 5 shows spectrum obtained from an unbiased device. The peaks in the scan of intensity vs wavelength are caused by band emission from excited nitrogen molecules. The positions of the known bands are identified in the figure. The close agreement between the observed peaks and the known positions of the nitrogen bands is evidence that arcing occurs between electrodes on the surface of the chip. A micrograph of the damaged region showed signs of mild heating but no anode-cathode pits commonly associated with arcs between electrodes in air. We surmised that rf joule heating of the material in the high-field region of the gate neck encouraged field emission of electrons lasting for some fraction of the rf pulse.

Figure 6 shows the history of the rectified second harmonic emitted from the input port of the device on two successive shots: the pulse preceding the damaging pulse,

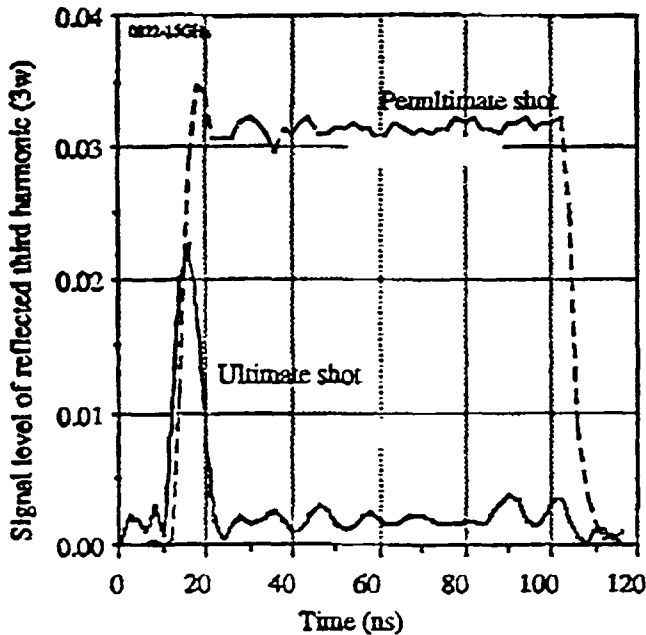


Figure 6

Second harmonic production during the damaging test and during the preceding test. The vanishing of the second harmonic is the signature of rectification failure.

and the damaging pulse itself. Prior to damage, the amplitude of the harmonics are proportional to that of the fundamental, but on the damaging shot, the harmonics vanish early while the fundamental continues on. This is the signature of rectification failure. Harmonics are generated by the clipping action of the gate junction which acts as a diode alternately driven into forward conduction during the forward half cycle and into avalanche breakdown during the reverse half cycle. When the junction ceases to act as a diode, the clipping action ceases and the harmonics vanish. Microscopically, the cause of rectification failure is still unknown. The junction metallurgy may be altered by heating or the phenomenon may be related to a type of current mode second breakdown observed by Van Lint et al.<sup>8</sup>. This year we have plans to study both possible causes: the metallurgy, using tunneling electron spectroscopy, and the breakdown, using broad band video pulses in place of the rf pulses used in the previous experiments.

While these studies are in progress, we are ex-

ploiting the knowledgewe have gained on damage mechanisms by having some off-the-shelf MMIC amplifiers altered to withstand greater incident energy. This first generation of hardened devices is scheduled for testing in July of 1991.

#### REFERENCES

1. J. J. Whalen, M. C. Calcatea, and M. L. Thorn, "Microwave Nanosecond Pulse Burnout Properties of GaAs MEFETs," IEEE Transactions MTT-27, p. 1026-1031, December 1979.
2. D. S. James, and L. Dormer, "A Study of High Power Pulsed Characteristics of Low-Noise GaAs MESFETs," IEEE Transactions MTT-29, p. 1298-1310, December 1981.
3. W. T. Anderson, Jr., A. Christou, and B. R. Wilkins, "GaAs FET High Power Pulse Reliability," 21st Annual Proceedings on Reliability Physics, IEEE Press, p. 218-225, April 1983
4. A. A. Moulthrop, and T. T. Mori, "Electromagnetic Pulse Damage of Low-noise GaAs FETs," 1986 Military Communications Conference 4 43.2.1.
5. H. J. Finlay, L. D. Roberts, R. F. B. Conlon, and D. Standing, "Recent Developments in RF Overload Mechanisms, Burnout and Reliability of Low-noise GaAs FET Amplifiers," 14th European Microwave Conference 84, p. 404-409.
6. John H. McAdoo, W. M. Bollen, and R. Garver, "Single-Pulse RF Damage of GaAs FET Amplifiers," 1988 IEEE MTT-S Digest
7. W.T. Anderson, F.A. Buot, A. Christou, Y. Anand, "High Power Pulse Reliability of GaAs Power FETs," 24th Annual Proceedings on Reliability Physics, IEEE Press, p. 144-149, 1986.
8. Julie E. Lawrance, Victor A. J. van Lint, and James P. Raymond; "Investigation of Latchup in NPN Bipolar and N Channel MOS Devices," Proceedings of the High Energy and Radiation Technology (HEART) Conference, 1990.

## Rectification Failure in GaAs MESFETs Subjected to Single Pulses of Intense Microwave Radiation

John H. McAdoo, W. Michael Bollen, Robert Seeley, and Will Catoe  
Mission Research Corporation  
8560 Cinderbed Road  
Newington, VA 22122

Jeffrey Frey  
Department of Electrical Engineering  
University of Maryland  
College Park, MD 20742-3020

Rectification failure has been found to be a major high-power microwave failure mechanism in amplifiers employing gallium arsenide metal field effect transistors (GaAs MESFETs). The mechanism results in the destruction of the rectifying property of the Schottky junctions. A junction that has so failed can no longer block the flow of current in either direction and acts as an ordinary ohmic resistor. Catastrophic failure follows from current driven by bias voltages through the failed junction.

Previous investigators employing trains of lower power pulses had identified metal migration as a key failure mode for extended exposure to moderate levels of microwave radiation (1-5). However, we have found the failure signature to be different when damage is caused by single high power microwave pulses lasting for a time short compared to the thermal transfer time of a MESFET gate (6). In 1986 Anderson (7) described a single pulse failure mechanism called "subsurface burnout." He based his arguments on postmortem observations of the surfaces of the damaged devices.

Rectification failure differs significantly from subsurface burnout. We have identified rectification failure with a combination of diagnostic techniques never before brought to bear. High-speed photography was used to clock the emission of optical radiation after the arrival of the high power microwave pulse, optical spectroscopy was employed to determine the source of the optical emissions, and rf spectroscopy was applied to monitor the generation of harmonics of the incident radiation as a function of time during each test pulse. Devices tested included packaged low-noise amplifiers, and power amplifiers. The tests proceeded by the direct injection of a single pulse of microwave radiation into the input port of the device. The pulses typically lasted for 100 ns. Testing would start at power levels too low to inflict damage and would proceed with successively higher power pulses until damage was observed. Devices were tested both with and without bias voltages applied.

# ENHANCED RELIABILITY IN SI MOSFET'S WITH CHANNEL LENGTHS UNDER 0.2 MICRON

Lindor Henrikson, Zezhong Peng, Jeffrey Frey, Neil Goldsman  
Department of Electrical Engineering  
University of Maryland  
College Park, MD 20742

## ABSTRACT

Simulations of n-channel silicon MOSFET's with gate lengths between 0.05 and 0.25 microns, performed using a two dimensional self-consistent energy transport model, show that with constant-field scaling maximum electron temperature decreases significantly as channel length decreases for channel lengths less than 0.18 microns. This result, indicates that short-channel devices can be more reliable than similar long channel devices.

## INTRODUCTION

Reduction in MOSFET channel lengths and consequent increases in peak electric fields have led to reductions in device reliability through hot-electron effects such as threshold voltage shift and parasitic gate current. However, it is important to realize increases in electron energy require not only that high electric fields be present, but also that sufficient scattering events occur to randomize electron momentum and/or energy. As channel lengths are shortened, chances that such interactions are "sufficient" are reduced, and for a given field, electrons in a shorter device may acquire less energy—i.e. become less "hot"—than electrons in a longer device. In fact, recent experimental results indicate<sup>1</sup> that hot-electron induced substrate current in Si MOSFET's is reduced with channel lengths less than 0.15 micron. Therefore, the hot-electron reliability problem may not monotonically become more severe as channel lengths are decreased.

In order to verify this apparent shorter-channel benefit, and to quantify where beneficial results might be expected, we have investigated the behavior of n-channel silicon MOSFET's with gate lengths under 0.25 micron, using techniques which yield true electron energies. These techniques are very efficient, consuming only a few minutes of SUN 3/60 cpu time per device bias point. Thus, submicron device reliability predictions can be made using an engineering workstation.

## THEORETICAL TECHNIQUES

N-channel silicon MOSFET's with channel lengths between 0.05 and 0.25 micron were simulated using the program UDMFET.<sup>2,3</sup> UDMFET self-consistently solves the Poisson, continuity, and energy balance<sup>4</sup> equations in two dimensions. Changes in electron energy due to acoustic and optical phonon scattering, heat flow, and diffusion are included.

The devices in our computer experiment were designed so as to keep the magnitude and shape of the lateral electric field the same in all. Doping concentrations and bias voltages on the gate and drain were therefore adjusted, as shown in Table 1. A maximum lateral electric field of 200KV/cm was imposed on all devices. The gate and drain bias voltages for each device were kept almost equal so that the transverse electric field was negligible in comparison to the lateral electric field near the drain, where the electrons reach their maximum temperature. The ambient temperature for all of the devices simulated was 300K.

## RESULTS

Sample profiles for lateral electric field at the surfaces of three of the simulated devices, and the resulting curves of surface electron temperature as a function of distance from the drawn gate edge, are shown in Figure 1. The results are summarized in Figure 2. These results show that for channel lengths below 0.18 micron the maximum electron temperature, related to the maximum energy available to cause reliability problems, decreases as channel length is decreased. For channel lengths above 0.18 micron the maximum electron energy changes little. For very long channels electron temperature is expected to approach a maximum value around 4300K, the temperature reached in a constant 200KV/cm field.<sup>5</sup>

## DISCUSSION

The electron temperature shown in Figures 1 and 2 is an average quantity which is a measure of the "randomness" of the electron energy, i.e., the spread of electron energies around an average value. Thermalization, an increase in this randomness, is caused by scattering events as the electrons travel through the device. A higher electron temperature at any point implies that more electrons have undergone randomizing collisions up to that point. Some of the electrons may have, on balance, acquired energy from the lattice; some may have lost it. Electrons with energies larger than the lattice temperature are "hot". If hot enough, these electrons cause reliability problems. In any case, the average electron temperature (plotted in Figs. 1 and 2) is an indicator of the spread of energies to be found in the electrons; the larger this spread, the greater the number of hot electrons.

In a MOSFET electrons are accelerated by the lateral electric field over the length of the channel. If the channel is very short, the field has only a limited time to act on the electrons, and the electrons can suffer only a relatively few randomizing collisions. However, as channel length is increased, the electrons have time to reach a maximum value of energy (i.e., the range of energies which they exhibit reaches some equilibrium value). Figure 2 shows that this critical length is around 0.18 micron for the field profiles we have used. This is also the value of channel length at which velocity overshoot, a related effect, has been shown to appear in short-channel MOSFET's.<sup>6</sup> A more complete discussion of the relationship of electron temperature to device reliability has been given elsewhere.<sup>7</sup>

## CONCLUSIONS

In very short-channel devices, the transit time of electrons through the high electric field may be shorter than the energy relaxation time. When this happens, the electrons do not have enough time to fully exchange energy with the lattice. The result is a lower average electron temperature than would occur in a similar long-channel device. Hot-electron related MOSFET reliability problems should therefore become less threatening for silicon MOSFET's with very short channel lengths, even if the electric fields and drain-source voltages in these devices remain relatively high. For devices scaled as those here, improvements should be noticed for channel lengths under about 0.18 micron.

We would like to thank T. Urai for his help with UMDFET and many discussions on electron transport phenomena.

### REFERENCES

- [1] G.G. Shahidi, D.A. Antoniadis, and H.I. Smith, "Reduction of Channel Hot-Electron-Generated Substrate Current in Sub-150nm Channel Length Si MOSFET's," *IEEE Electron Device Letters*, vol. 9, p. 497, 1988.
- [2] Z. Peng, "UMDFET A Two-dimensional General Device Simulator and its Application in EPROM Analysis," Master's Thesis, 1989, in the University of Maryland.
- [3] Z. Peng and J. Frey, "Facilitating Convergence in EPROM Device Simulation," Digest of the NASECODE VI Software Forum, 1989.
- [4] R.K. Cook and J. Frey, "An Efficient Technique for Two-dimensional Simulation of Velocity Overshoot Effects in Si and GaAs Devices," *Compel.*, vol. 1, p. 65, 1982.
- [5] C. Jacoboni and L. Reggiani, "The Monte Carlo Method for Solution of Charge Transport in Semiconductors with Applications to Covalent Materials," *Rev. of Modern Phys.*, vol. 55, p. 645, 1983.
- [6] G. Sai-Halasz, M. Wordeman, D. Kern, S. Rishton, and E. Ganin, "High Transconductance and Velocity Overshoot in NMOS Devices at the 0.1-micron Gate-length Level," *IEEE Electron Device Letters*, vol. 9, p. 464, 1988.
- [7] J. Frey and N. Goldsman, "Tradeoffs and Electron Temperature Calculations in Lightly Doped Drain Structures," *IEEE Electron Device Letters*, vol. 6, no. 1, p. 28, 1985.

L	Nd	Na	xj	tox	Vg	Vd
0.05	2.90e19	2.36e16	0.013	20	0.30	0.32
0.08	2.70e19	2.36e16	0.013	25	0.60	0.56
0.10	3.00e19	2.36e16	0.018	25	0.64	0.65
0.15	3.00e19	3.47e16	0.018	25	0.90	0.83
0.18	3.00e19	3.47e16	0.018	25	0.98	0.90
0.25	5.90e19	2.64e16	0.038	25	1.50	1.45

L=gate length

Nd=max. doping concentration at drain and source (cm<sup>-3</sup>)

Na=implant concentration in channel (cm<sup>-3</sup>)

xj=drain and source junction depths (micron)

tox=oxide thickness (nm)

Vg=gate bias (V)

Vd=drain bias (V)

Vs=Vb=0.0, where Vs and Vb are the bias voltages of the source and bulk (Device doping profiles obtained using process simulator from MINIMOS. Drain and source junctions are diffused As, channels are B ion implants)

Table 1. Device parameters of the simulated MOSFET's.

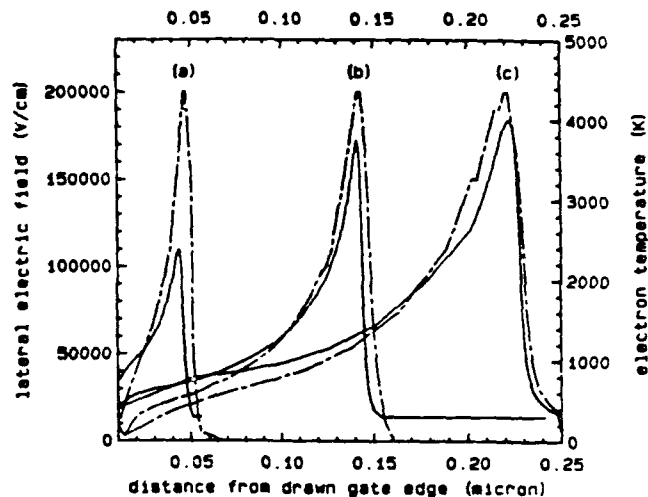


Figure 1. Lateral electric field (long dash short dash) and electron temperature (solid) profiles vs. distance from drawn gate edge for (a) 0.05 micron gate length, (b) 0.15 micron gate length, and (c) 0.25 micron gate length n-channel silicon MOSFET's.

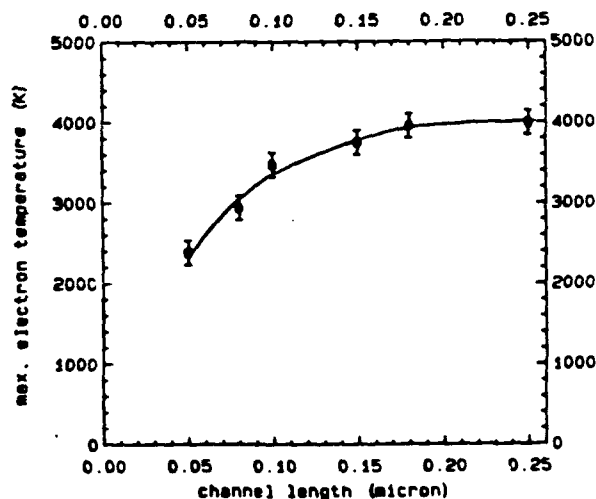


Figure 2. Maximum electron temperature at surface of channel vs. channel length for 0.05, 0.08, 0.1, 0.15, 0.18, and 0.25 gate length n-channel silicon MOSFET's with peak lateral electric field of 200KV/cm. Error bars of +/-150K reflect uncertainties in scattering parameters and simulation program convergence tolerances.

## **Efficient calculation of ionization coefficients in silicon from the energy distribution function**

Neil Goldman, Yu-Jen Wu, and Jeffrey Frey

*Department of Electrical Engineering, University of Maryland, College Park, Maryland 20472*

(Received 6 November 1989; accepted for publication 20 April 1990)

A method for calculating impact ionization coefficients by solving the Boltzmann transport equation is presented. The distribution function is taken to be expressible as a Legendre polynomial expansion, which is substituted into a Boltzmann equation that incorporates the effects of nonparabolic band structure, deformation-potential phonon scattering, and impact ionization. The resulting Boltzmann equation can be expressed in a linear form, and solved using sparse-matrix difference-differential methods. Ionization coefficients are obtained directly from the distribution function. Calculated values for the ionization coefficients agree very well with experiment for electrons in silicon.

# RELY: A PHYSICS-BASED CAD TOOL FOR TIME-DEPENDENT HOT-ELECTRON INDUCED MOSFET RELIABILITY INVESTIGATIONS

Shiuh-Luen Wang, Neil Goldman, and Jeffrey Frey

Department of Electrical Engineering, The University of Maryland  
College Park, MD 20742, U.S.A.

RELY, a new MOSFET simulator for predicting hot-electron induced degradation problems is presented. RELY uses the distribution function calculated by solving the Energy and Boltzmann transport equations to allow prediction of the time dependence of gate-leakage current, oxide charge deposition, and device I-V characteristics. Results agree with experiment and Monte Carlo calculations, and are obtained in only several CPU minutes.

## INTRODUCTION

We present here RELY, a novel, physics-based CAD tool for predicting MOSFET reliability problems. As device dimensions continue to shrink, many forms of device degradation will be prevalent. Gate-leakage current, threshold voltage shifts, and transconductance shifts, arising from hot-electron damage, are particularly threatening, these phenomena degrade device operating characteristics over time, and may ultimately lead to device failure. Models previously proposed for predicting reliability problems, including the popular Richardson's Equation Method for emission over a barrier, are often based on the incorrect assumption that the electron distribution function is Maxwellian [1]. Other methods, including Monte Carlo simulation, are more physically rigorous, but require prohibitive amounts of CPU time, and are thus inappropriate for use in most CAD tools for predicting device reliability [2].

The new device reliability simulator, RELY, is both physics-based, and computationally efficient. RELY uses a new, Energy Transport-Boltzmann Transport Equation (ET-BTE) model. Since RELY is physics-based, the need for many fitting parameters, often associated with predicting device degradation, is eliminated. The ET-BTE model uses real device physics - scattering mechanisms and nonparabolic band structure - to calculate the average electron energy and the electron distribution function throughout a device. By utilizing this information, RELY predicts MOSFET gate-leakage current and threshold voltage shift to ascertain their effects on device operation as a function of stressing time. Excellent agreement with experiment is attained; calculations have also been shown to agree with Monte Carlo simulations while requiring less than 1/100 the CPU time to evaluate.

## MODEL DESCRIPTION

### ET-BTE Model

The ET-BTE model consists of five equations: the Energy Transport equation (ET) (1), and the Boltzmann Transport equation (BTE) (2), as well as the Poisson (3), continuity (4) and current (5) equations.

$$\frac{3}{5} \nabla \cdot (n v \omega) = -e n v \cdot E + n \frac{\omega - \omega_0}{\tau_{\omega}(\omega)} \quad (1)$$

$$\frac{E}{\hbar} E_{eff} \nabla_k f(k) = \left[ \frac{\partial f(k)}{\partial t} \right]_{ac} + \left[ \frac{\partial f(k)}{\partial t} \right]_{iv} \quad (2)$$

$$\nabla \cdot \nabla \psi + (e/\epsilon) (p - n + N) = 0 \quad (3)$$

$$\nabla \cdot J_n = eR \quad (4)$$

$$J_n = -e (\mu_n n \nabla \psi - D_n \nabla n) \quad (5)$$

where  $\psi$  is the electrostatic potential,  $n$  and  $p$  are electron and hole concentrations,  $N$  is the net fixed charge density,  $R$  is the net recombination rate,  $J_n$  is the electron current density ( $J_n = -en v$ ).  $v$ ,  $\omega$ ,  $E$ ,  $f(k)$ ,  $E_{eff}$ ,  $\tau_{\omega}$ , and  $k$ , are the electron average velocity, electron average energy, electric field, distribution function, effective electric field, energy relaxation time and wave vector respectively. The subscripts  $ac$  and  $iv$  in the BTE represent the effects of acoustic and intervalley phonon scattering on the distribution function.

To facilitate predicting time-dependent device reliability problems, RELY calculates the change in currents and electrostatic potential due to hot-electron degradation as a function of operation time. To begin these calculations, the initial values (time  $t=0$ ) for electrostatic potential and carrier concentrations are provided by a 2-D Poisson-continuity equation solver, such as MINIMOS [3]. With concentration and potential as input, RELY then solves the energy balance equation (1) in two dimensions. To solve equation (1), a finite difference (FD) scheme is applied. Discretization is performed at boundary elements by modification of the FD formulae using the mirror image technique [4]. This technique provides more accurate use of equation (1) by eliminating the typical requirement that carrier and lattice temperatures be equal at the boundaries. Finally, a constant value for energy relaxation time, shown by Monte Carlo calculations to be  $2.6 \times 10^{-13}$  sec, is used [5]. The solution of equation (1) provides the average electron energy as a function of the device's space coordinates. Device regions of high electron energy are potential problem areas.

To find the distribution function at each channel coordinate, the average energy found above is used in conjunction with solutions to the homogeneous-field Boltzmann Transport Equation (2). Due to its complexity, we present here only a symbolic representation of the BTE. Within RELY, the homogeneous-field BTE is formulated using Legendre polynomials, while accounting for the effects of silicon's

nonparabolic band structure, intervalley and acoustic phonon scattering [6]. The details of the phonon collision integrals are expressed in terms of deformation potential scattering theory. Values for deformation potentials are identical to those used for Monte Carlo calculations [7]. To account for space dependence an effective electric field  $E_{eff}$  is used as input to equation (2).

$E_{eff}$  is obtained by mapping position-dependent average energy, found from the solution to equation (1), to the corresponding electric field on the homogeneous-average-energy versus electric-field curve. This curve was calculated by Monte Carlo analysis beforehand. After inputting  $E_{eff}$ , RELY numerically solves the BTE using the finite difference method.

The solutions to the above five equations provide the average energy and the electron distribution function throughout the device, as well as the I-V characteristics.

### Gate-Leakage Current

MOSFET gate leakage current appears when electrons gain enough energy to surmount or tunnel through the oxide barrier. The magnitude of thermally-emitted gate-leakage current is given by the number of electrons which are energetic enough to surmount the oxide barrier, multiplied by their respective velocities in the direction of the oxide. Mathematically this is given as

$$J_g(x) = \int_{k_0}^{\infty} e n(x) v_z(k) F(x, k) d^3k \quad (6)$$

where  $J_g(x)$  is the gate current density,  $n(x)$  is the electron concentration,  $k_0$  is the minimum electron wave vector necessary for surmounting the oxide barrier,  $v_z(k)$  is the electron velocity perpendicular to the interface,  $F(x, k)$  is the space-dependent momentum distribution function.

By performing a great deal of algebraic manipulations, which are made difficult by silicon's ellipsoidal, nonparabolic band structure, we convert the above equation to an explicit expression for calculating gate current density in MOSFETs [8]. This new expression is similar to Richardson's equation for thermal emission over a barrier. However, unlike Richardson's equation which is based on a Maxwellian, the new expression is derived from the physics-based hot-electron distribution function, which is found from the ET-BTE model described above. This new expression is

$$J_g(x) = \frac{2\pi e n(x)}{3\hbar^3} (m_t^2 m_l)^{1/2} \left[ \frac{1}{m_l^{1/2}} + \frac{2}{m_l^{1/2}} \int_{\phi_0}^{\infty} f(x, \epsilon) \gamma(\epsilon) d\epsilon \right] \quad (7)$$

where  $m_t$  and  $m_l$  are silicon's transverse and longitudinal effective masses respectively,  $\gamma(\epsilon)$  is silicon's nonparabolic dispersion relation [7],  $\phi_0$  is the oxide barrier height,  $f(x, \epsilon)$  is the space-dependent energy distribution function, which has units of  $cm^{-3}$ ; it gives the probability of finding an electron in the vicinity of energy  $\epsilon$  and location  $x$ .

The effects of Schottky barrier lowering and electron tunneling are accounted for by adjusting the oxide barrier height according to the following expression [9]:

$$\phi_0 = 3.1 - bE_{ox}^{1/2} - aE_{ox}^{1/2} \quad (8)$$

$E_{ox}$  is the electric field in the oxide.  $a$  and  $b$ , which have been determined by comparison with experiment, have the values  $1 \times 10^{-5} e(cm^2V)^{1/3}$  and  $2.6 \times 10^{-4} e(cmV)^{1/2}$  respectively.

RELY numerically integrates equation (7), while inserting proper values for  $f(\epsilon, x)$  determined by the ET-BTE method, to ascertain gate leakage current density as a function

of channel coordinate. Total gate-leakage current  $I_g$  is obtained by integrating  $J_g(x)$  along the channel:

$$I_g = W_g \int_{x_s}^{x_d} J_g(x) dx \quad (9)$$

$W_g$  is the width of the MOSFET gate.  $x_s$  and  $x_d$  are the source and drain coordinates respectively.

### Oxide Charge Buildup and Device Degradation in Time

A small fraction of the hot electrons which surmount the oxide barrier become trapped in oxide states. The oxide charge deposition gives rise to higher channel resistivity and increased threshold voltage, and ultimately affects the basic I-V characteristics of the device. RELY predicts time-dependent oxide charge buildup by using the following equation which describes the exponential relationship between the occupation of oxide states, the gate current density, and the device stressing time [9]:

$$N_{ox}(t) = \sum_i N_{oxi} \left[ 1 - \exp\left(-\frac{J_g(x) \sigma_i}{e}\right) \right] \quad (10)$$

where  $N_{oxi}$  is the density of type  $i$  oxide traps,  $N_{ox}(t)$  is the number of oxide states filled at time  $t$ ,  $\sigma_i$  is the cross section of oxide trap  $i$ .

Using the previously calculated gate current density, RELY evaluates equation (10) to predict values for oxide charge accumulation with time. The default values for trap densities and cross sections are [10]

$$\sigma_1 = 1.71 \times 10^{-17}, \sigma_2 = 8.81 \times 10^{-17}, \sigma_3 = 1.93 \times 10^{-16}$$

$$N_{ox1} = 9.65 \times 10^{11}, N_{ox2} = 9.43 \times 10^{11}, N_{ox3} = 1.14 \times 10^{12}$$

The trapped charge distributions in the oxide often cause a localized perturbation on the potential and carrier distributions near the drain region of the device. This perturbation potential is determined in two dimensions using the time perturbation method [11]. At time  $t_1$ , the Poisson's equation can be written as

$$\nabla \cdot \nabla \phi(x, y, t_1) = \rho(x, y, t_1) / \epsilon_{ox}, \quad \text{in oxide} \quad (11)$$

$$\nabla \cdot \nabla \phi(x, y, t_1) = e(n' - p' - N) / \epsilon_s, \quad \text{in silicon} \quad (12)$$

where  $f(x, y, t_1)$  is the new potential because of the perturbation caused by the trapped charges,  $n'$  and  $p'$  are the new electron and hole concentrations,  $\rho(x, y, t_1)$  ( $= e N_{ox}(x, y, t_1)$ ) is the trapped oxide charge calculated above.

The new potential can be decomposed into a time independent part and a time dependent part. At time  $t_1$ ,

$$\phi(x, y, t_1) = \psi(x, y) + u(x, y, t_1) \quad (13)$$

where  $u(x, y, t_1)$  is the perturbation potential at time  $t_1$ .

We start with a potential distribution and electron concentrations obtained from MINIMOS. Then, the perturbation potential is obtained after substituting relation (13) into (11) and (12), and linearizing the resulting equations. After the perturbation potential is determined, local corrections are made to the carrier concentrations. In time, as more charge becomes trapped in the oxide, we periodically use the perturbation method to re-evaluate the Poisson and continuity equations. At each iteration, the new I-V characteristics and threshold voltage shift are calculated using the updated potential distributions and charge concentrations. The flow diagram of RELY is shown in Figure 1.

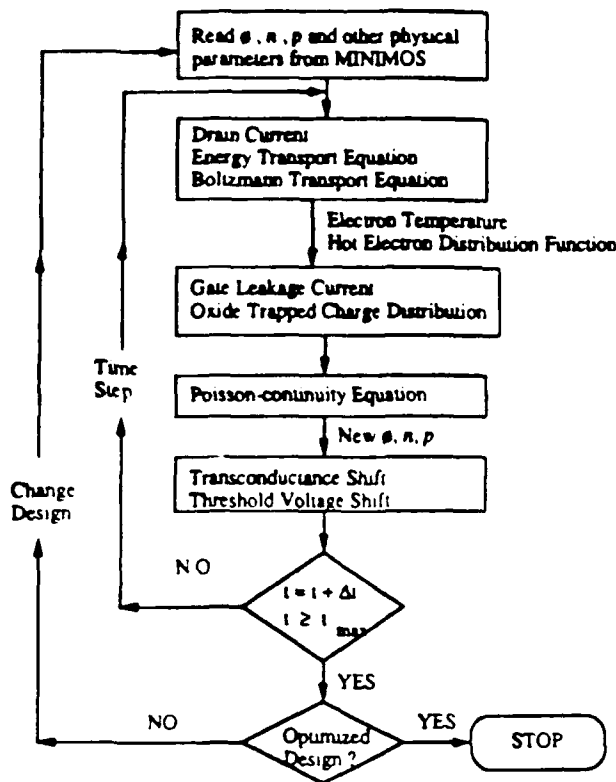


Figure 1 The Flow Diagram of RELY

## RESULTS AND DISCUSSIONS

To demonstrate the capabilities of RELY, we simulated n-channel MOSFETs on a SUN desktop computer. Figure 2 shows energy versus position along the channel; areas of large electron energy indicate regions subject to increased degradation. Figure 3 compares distribution functions calculated by RELY (Legendre polynomial technique), the Monte Carlo method, and the Maxwellian distribution. While there is good agreement between Legendre polynomial and Monte Carlo techniques, the Maxwellian disagrees significantly over all energies. Such agreement between Monte Carlo and Legendre polynomial techniques indicates that the new ET-BTE method does indeed predict realistic values for distribution function. RELY predicts values for gate current which match very well with experiment for over four order of magnitude as shown in Figure 4. Unlike other models, which ignore the actual physical mechanisms, RELY attains agreement for a wide range of bias conditions, using the poorly-known phonon deformation potential as its only adjustable parameter. When more reliable values for these phonon-electron coupling factors are available, we are likely to render unnecessary the one fitting parameter currently required by RELY for gate current predictions. Figure 5 compares oxide charging of the test device after operation times of 0.01, 1.0, and 100 hours. Reasonable values for temporal evolution of drain current have also been obtained as shown in Figure 6. The presented method of oxide charging has also been applied to simulate EPROM programming characteristics and excellent agreement with experiment has been obtained as shown in Figure 7 [12].

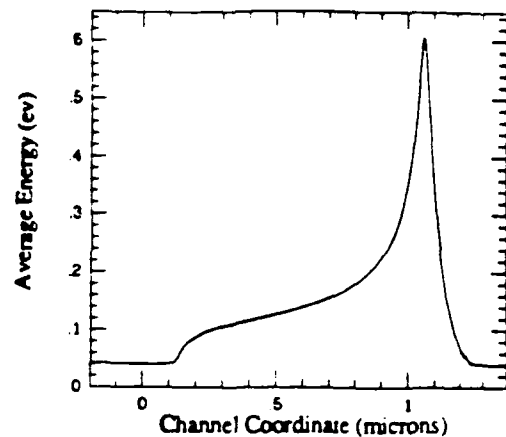


Figure 2 Average energy versus position along the channel. The device is biased at  $V_{ds}=6.0V$  and  $V_{gs}=7.0V$ .  $L/W = 1.2\mu m / 50.8\mu m$ ,  $t_{ox} = 150\text{\AA}$ . Gate oxide begins at  $x=0$ .

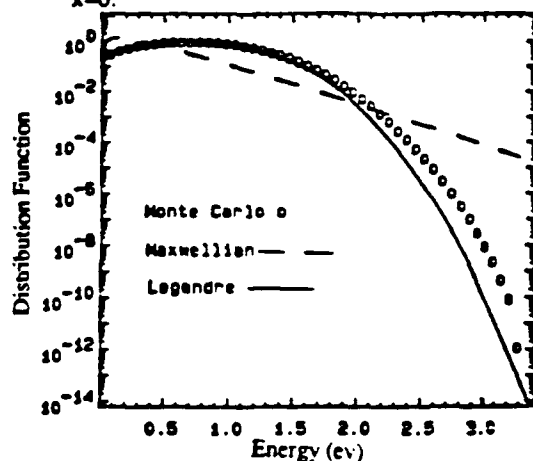


Figure 3 The Legendre polynomial distribution function and Maxwellian distribution are compared with the distribution function calculated using Monte Carlo technique. All distributions are for an average energy of  $0.72\text{ev}$ .

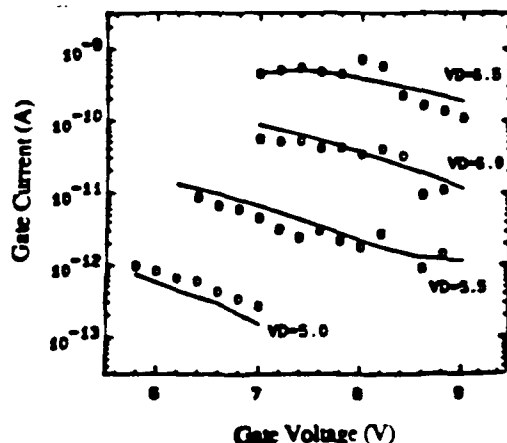


Figure 4 Gate current versus gate voltage. Open circles are calculated with RELY; the solid lines are experimental values.  $L/W = 1.2\mu m / 50.8\mu m$ ,  $t_{ox} = 150\text{\AA}$ .

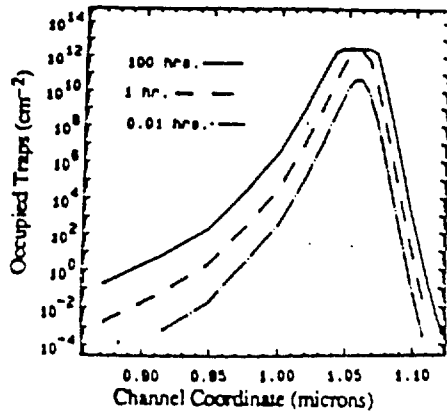


Figure 5 Oxide filling is compared after 0.01, 1.0, and 100 hours of operation.

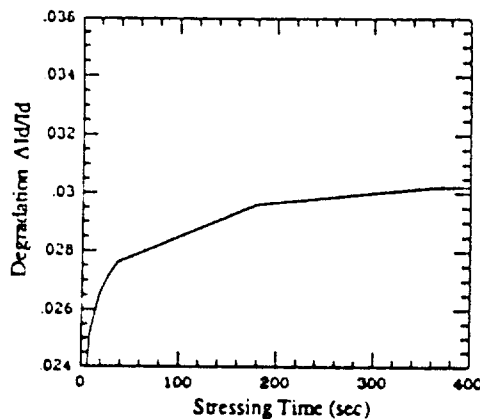


Figure 6 Calculated drain current degradation ( $\Delta I / I$ ) versus stressing time. Stress condition is  $V_{ds}=8.0V$  and  $V_{gs}=3.0V$ . The characterization is with  $V_{ds}=0.1V$  and  $V_{gs}=3.0V$ .  $L/W = 0.6\mu m / 50.8\mu m$ ,  $t_{ox} = 150\text{\AA}$ .

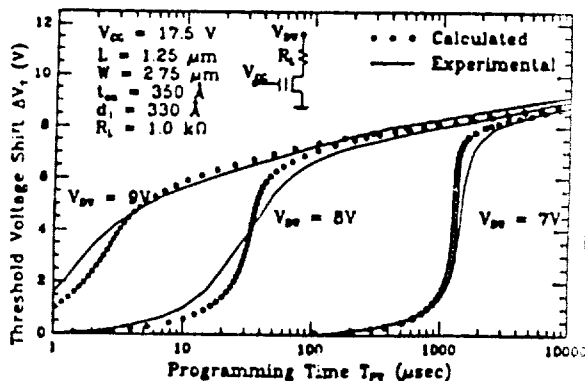


Figure 7 The presented method of oxide charging has been applied to simulate EPROM programming and excellent agreement with experiment has been obtained [12].

## CONCLUSION

RELY, a CAD tool which combines physics engineering practicality, has been developed. minutes of calculation on a work-station compute simulate time-dependent, hot-electron induced problems, as well as mean time to failure, in de fabricated. Such simulations should prove va design of reliable submicron semiconductor device

## ACKNOWLEDGEMENTS

This work was supported in part by: the Se Research Corporation U.S.A.; the Manta Martin Fu the University of Maryland U.S.A.; and the U.S. Science Foundation under grant number ECS-9010.

## REFERENCES

- [1] E. Takeda, H. Kume, T. Toyabe and "Submicrometer MOSFET structure for Minir carrier Generation," *IEEE Tran. Electron Devi* PP. 611-618, 1982.
- [2] Jeffrey Yuh-Fong Tang, "Theoretical Studie. Field, High Energy Transport in Gallium Silicon and Heterostructure," Ph.D. Thesis, Un Illinois, 1983.
- [3] S. Selberherr, A. Schutz, H.W. Poizl, "MINI Two-Dimensional MOS Transistor Analyzer," *II Electron Devices*, ED-27, pp. 1540-1550, 1980.
- [4] C. McAndrew, E.L. Heasell, and K. Singhal, "Dynamical VLSI Device Simulation," *Semic. Science Technology*, 3, pp. 886-894, 1988.
- [5] N. Goldsman, J. Frey, "Efficient and Accurate L Energy Transport Method in Device Simulation," *Tran. Electron Devices*, ED-35, pp. 1524-1529, 1
- [6] N. Goldsman, L. Henrickson, J. Frey, "A Physic Analytical/Numerical Solution to the Boltzmann 1 Equation for Use in Device Simulation," to be p in *Solid-State Electronics*.
- [7] C. Jacoboni and L. Reggiani, "Monte Carlo Met the solution of Charge Transport in Semiconduct Applications to Covalent Materials," *Reviews of A Physics* 55, pp. 645-705, 1983.
- [8] N. Goldsman, "Modeling Electron Transpo Degradation Mechanisms in Semiconductor Sub Devices," Ph.D. Thesis, Cornell University, 1989.
- [9] T.H. Ning and H.N. Yu, "Optically Induced Injec Hot Electrons into  $SiO_2$ ," *J. Appl. Phys.* 45, pp. 5378, 1974.
- [10] R.F. De Keersmaecker, "Charge Trapping in *Insulating Films on Semiconductors*, ed. D.R. W pp. 85-97, 1983.
- [11] R. Rakkhit, M.C. Peckerar, C.T. Yao, "An Investi of the Time Dependence of Current Degradation in Devices," *Proceedings of the International Relia Physics Symposium*, pp. 103-109, 1989.
- [12] T. Urai, Z.Z. Peng, J. Frey, N. Goldsman, "Simulati EPROM Programming Characteristics," *Workshop Numerical Modeling of Processes and Devices Integrated Circuits (NUPAD III)*, June 3, 1990.

Reproduced From  
Best Available Copy

## MOSFET HOT-ELECTRON GATE CURRENT CALCULATION BY COMBINING ENERGY TRANSPORT METHOD WITH MONTE CARLO SIMULATION

Shiuh-Luen Wang, Neil Goldsman, Lindor Henrickson, and Jeffrey Frey

Department of Electrical Engineering, University of Maryland  
College Park, MD 20742, U.S.A.

### ABSTRACT

This paper describes a novel technique, which combines the attributes of the Energy Transport and Monte Carlo methods, for determining MOSFET gate current that arises from electron heating in the device. This method is based upon a non-Maxwellian hot-electron distribution function found from Monte Carlo simulation, and utilizes a physically-calculated average electron energy. Calculated values for gate current of a sample submicron MOSFET device show reasonably good agreement with experiment without the need for any fitting parameters.

### INTRODUCTION

Hot electron injection into the gate oxide is the underlying mechanism largely responsible for MOSFET gate leakage current, MOSFET performance degradation, and EPROM programming. To accurately investigate these hot-electron phenomena, the energy distribution function is needed. However, neither the conventional Drift-Diffusion (DD) model nor the more complex Hydrodynamic Energy Transport (ET) model provide the distribution function. Therefore, much effort has been invested in predicting oxide injection. Many models previously proposed, including the popular Richardson's Equation method [1,2], are based on the disputed assumption that the distribution function is Maxwellian. Other approaches do not make such an assumption, but are computationally too expensive to be of day-to-day use for device design [3].

In this paper we present a novel technique, which couples the Energy Transport and the Monte Carlo (MC) methods, to determine oxide injection and MOSFET gate current. The merits of this new Energy Transport-Monte Carlo (ET-MC) approach are: (1) it incorporates the semiconductor band structure and scattering mechanisms; (2) it requires less CPU time than a standard MC analysis; (3) it uses a robust distribution function tail population-enhancement scheme; (4) it is a candidate for CAD applications.

### ET-MC MATHEMATICAL MODEL

The ET-MC is composed of a homogeneous-field Monte Carlo calculation in conjunction with the Poisson (1), continuity (2), current (3), and energy balance (4) equations.

$$\nabla^2\psi + \frac{e}{\epsilon_s}(p - n + N) = 0 \quad (1)$$

$$\nabla \cdot J_n = eR \quad (2)$$

$$J_n = -e(\mu_n n \nabla \psi - D_n \nabla n) \quad (3)$$

$$v \cdot \nabla \omega = e(v \cdot E) - \frac{2}{3n} \nabla \cdot (n v \omega) + \left. \frac{\partial \omega}{\partial t} \right|_{coll} \quad (4)$$

where  $n$ ,  $p$ ,  $J_n$ ,  $v$ ,  $\omega$ ,  $E$ ,  $R$ ,  $\mu_n$ , and  $D_n$  are the electron concentration, hole concentration, electron current density, electron drift velocity, electron average energy, electric field, recombination rate, mobility and diffusion coefficient respectively.

### ET-MC ALGORITHM

To evaluate the mathematical model described above, we perform the following operations.

1. The electrostatic potential and carrier concentrations within the device are calculated by a 2-D Poisson-continuity equations solver, such as MINIMOS or UMDFET [4,5].
2. The average electron energy as a function of device's space coordinates is obtained by solving energy balance equation (4) using the algorithm described in reference [6]. The electric field obtained from the above Poisson-continuity solver is used as input to equation (4).
3. An *effective-electric field profile* is then determined to facilitate determining the space-dependent distribution function.
4. The space-dependent distribution function is ascertained using homogeneous-field MC simulations with the effective field as input.
5. The gate current density is found by employing thermionic emission arguments while using the newly-calculated distribution function.

The novelty of this work is contained in steps 3 through 5 which are described in detail below.

### Effective-Electric Field Profile

To account for the effects of nonlocal phenomena we define an effective-electric field profile. We determine the effective-electric field by mapping the average energy to the corresponding electric field on the homogeneous-electric field versus average energy curve, which is shown in Figure 1. After performing this operation for each space coordinate, an effective field profile is obtained. The space-dependent average energy has already been found from the solution of energy balance equation (4), while the homogeneous-electric field versus average energy curve was calculated by MC analysis beforehand. The effective and the actual electric field profiles in the channel, parallel to the interface, are shown in Figure 2.

### Space-Dependent Distribution Function

For phenomena which occur in silicon on the time scale of the energy relaxation time, the average electron energy is an accurate parameter to use as a guideline for interpolating homogeneous-field phenomena to space-dependent phenomena [7]. We utilize this concept to determine the space-dependent distribution function from homogeneous-field MC calculations. More specifically, we first determine points where average energy is greatest. We then perform homogeneous-field MC simulations at each of those points using the effective-electric field values as input.

### Calculating the High-Energy Tail of the Distribution Function

To obtain the tail of the distribution function, where the occupation probability is very small, we divide our energy domain into high and low regions. We first generate a distribution in the low energy region where electron states are easily accessed. Once this region is statistically well defined, i.e., enough events have occurred to make the curve that is well defined, or smooth around this point, we need not generate any more events in this region, it is considered known. Now we start the electrons at the next energy region. This region begins at the highest energy point where this initial distribution function is well defined. We let this stage of the Monte Carlo proceed as usual, but when the electron energy falls below the energy breakpoint we have picked, it is thrown away and another electron is started again at this breakpoint. The part of the distribution function generated by this sequence of events must now be properly weighted with respect to the initial distribution function. This is easily done, because we already know the 'correct' probability of an occurrence at the energy breakpoint from the initial distribution function. Thus, we match values for the distribution function at the breakpoint. This matching is accomplished by multiplying all of the probabilities in the low probability region by a single weighting factor. We can extend the distribution function to higher and

higher energies, or lower and lower probability regions, by iterating this scheme many times.

This process may be more easily understood in mathematical terms. If  $N_1(\epsilon)$  is the occupation number in the initial easily-generated energy histogram at an energy  $\epsilon$ ,  $N_2(\epsilon)$  is the number obtained at energy  $\epsilon$  in the tail, and  $\epsilon_i$  is an energy breakpoint, then the weighting at each energy breakpoint is performed as follows:

1. For  $\epsilon \geq \epsilon_i$

$$N(\epsilon) = N_1(\epsilon) + N_2(\epsilon) \quad (5)$$

2. For  $\epsilon \geq \epsilon_i$ , multiply each such  $N(\epsilon)$  by the weighting factor

$$W(\epsilon_i) = \frac{N_1(\epsilon_i)}{N_1(\epsilon_i) + N_2(\epsilon_i)} \quad (6)$$

3. The unnormalized distribution function is then given by

$$F(\epsilon) = N_1(\epsilon) \quad \epsilon \leq \epsilon_i \quad (7a)$$

$$F(\epsilon) = N(\epsilon)W(\epsilon) \quad \epsilon \geq \epsilon_i \quad (7b)$$

### Gate-Leakage Current Calculation

MOSFET gate leakage current appears when electrons gain enough energy to surmount or tunnel through the oxide barrier. The magnitude of thermally-emitted gate-leakage current is given by the number of electrons which are energetic enough to surmount the oxide barrier, multiplied by their respective velocities in the direction of the oxide. Mathematically this is given as

$$J_g(x) = \int_{k_0}^{\infty} en(x)v_z(k)F(x,k)d^3k \quad (8)$$

where  $J_g(x)$  is the gate current density,  $n(x)$  is the electron concentration,  $k_0$  is the minimum electron wave vector necessary for surmounting the oxide barrier,  $v_z(k)$  is the electron velocity perpendicular to the interface,  $F(x,k)$  is the space-dependent momentum distribution function.

By performing a great deal of algebraic manipulations, which are made difficult by silicon's ellipsoidal, nonparabolic band structure, we convert the above equation to an explicit expression for calculating gate current density in MOSFETs [8]. This new expression is similar to Richardson's equation for thermionic emission over a barrier. However, unlike Richardson's equation which is based on a Maxwellian, the new expression is derived from a physics-based hot-electron distribution function, which is found from the ET-MC simulation described above. This new expression is

$$J_g(x) = \frac{2\pi en(x)m_1 m_1^{1/2}}{3\pi^3} \left[ \frac{1}{m_1^{1/2}} + \frac{2}{m_1^{1/2}} \right] \int_{\phi_B}^{\infty} f(x,\epsilon)\gamma(\epsilon)d\epsilon \quad (9)$$

where  $m_t$  and  $m_l$  are silicon's transverse and longitudinal effective masses respectively,  $\chi(\epsilon)$  is silicon's nonparabolic dispersion relation,  $\phi_B$  is the oxide barrier height.  $f(x, \epsilon)$  is the space-dependent energy distribution function, which has units of  $cm^{-3}$ ; it gives the probability of finding an electron in the vicinity of energy  $\epsilon$  and location  $x$ . The effects of Schottky barrier lowering and electron tunneling are accounted for by adjusting the oxide barrier height according to an empirically determined algorithm [9]. Values for  $J_g(x)$  are determined by integrating equation (9), while inserting proper values for  $f(x, \epsilon)$  determined by the ET-MC method. Total gate-leakage current  $I_g$  is obtained by integrating  $J_g(x)$  along the channel.

### RESULTS AND DISCUSSION

We demonstrate the new ET-MC method with a calculation of gate leakage current arising from an n-channel MOSFET with  $0.9\mu m$  effective gate length using a SUN desktop computer. The dispersion relation and scattering coupling factors are taken from reference [10]. Figure 3 shows energy versus position along the channel; areas of large electron energy indicate regions subject to increased degradation. The distribution function at channel coordinates  $1.045\mu m$  and  $1.061\mu m$ , corresponding to effective-electric field values of  $202kV/cm$  and  $237kV/cm$  are plotted in Figure 4. The excellent resolution in the high-energy region of the distribution function, demonstrated by the smooth curves in Figure 4, is attributable to the tail population-enhancement method discussed above. The electron energy distribution functions are multiplied by the density of states and normalized to unity. Values calculated for gate current using the presented ET-MC method and Richardson's equation are compared with experiment as shown in Figure 5. Figure 5 shows reasonably good agreement with experiment is obtained using the ET-MC method without the need for any fitting parameters; Richardson's method is in error by approximately 8 orders of magnitude. While reasonably good agreement with experiment was attained, we believe our method will be even more accurate when an even more detailed MC program is used. Furthermore, calculation times can be significantly reduced by providing a database of distribution functions, each corresponding to different effective field value.

### CONCLUSION

In sum, a new MOSFET gate injection current calculation method which combines the attributes of the MC and ET techniques is presented. Calculated values for gate current agree with experiment without the need of fitting parameters. The method allows for excellent resolution of the high-energy tail of the distribution function. Furthermore, the ET-MC model requires less CPU time than standard MC methods, and is therefore

appropriate for use in the computer aided design of semiconductor devices, especially after establishing a database of distribution functions.

### REFERENCES

- [1] E. Takeda, H. Kume, T. Toyabe, and S. Asai, "Submicrometer MOSFET Structure for Minimizing Hot-carrier Generation," *IEEE Trans. Electron Devices* ED-29 p. 611 (1982).
- [2] J. Frey and N. Goldsman, "Tradeoffs and Electron Temperature Calculations in Lightly Doped Drain Structures," *IEEE Electron Device Letters* EDL-6 p. 28 (1985).
- [3] Jeffrey Yuh-Fong Tang, "Theoretical Studies of High Field, High Energy Transport in Gallium Arsenide, Silicon and Heterostructures," Doctoral Thesis, University of Illinois (1983).
- [4] S. Selberherr, A. Schutz, and H. W. Potzl, "MINIMOS—A Two-Dimensional MOS Transistor Analyzer," *IEEE Trans. Electron Devices* ED-27 p. 1540 (1980).
- [5] Zezhong Peng, "UMDFET: A Two-Dimensional General Device Simulator and Its Application in EPROM Analysis," Masters Thesis, University of Maryland (1989).
- [6] N. Goldsman and J. Frey, "Efficient and Accurate Use of the Energy Transport Method in Device Simulation," *IEEE Trans. Electron Devices* ED-35 p. 1524 (1988).
- [7] E. E. Kunhardt, J. Wu, and B. Penetrante, "Nonequilibrium Macroscopic Descriptions of Electrons in Weakly Ionized Gases," *Physical Review A* 37 p. 1654 (1988).
- [8] Neil Goldsman, "Modeling Electron Transport and Degradation Mechanisms in Semiconductor Submicron Devices," Doctoral Thesis, Cornell University (1989).
- [9] T.H. Ning and H.N. Yu, "Optically Induced Injection of Hot Electrons into SiO<sub>2</sub>," *J. Appl. Phys.* 45 p. 5373 (1974).
- [10] C. Jacoboni and L. Reggiani, "Monte Carlo Method for the Solution of Charge Transport in Semiconductors with Applications to Covalent Materials," *Reviews of Modern Physics* 55 p. 645 (1983).

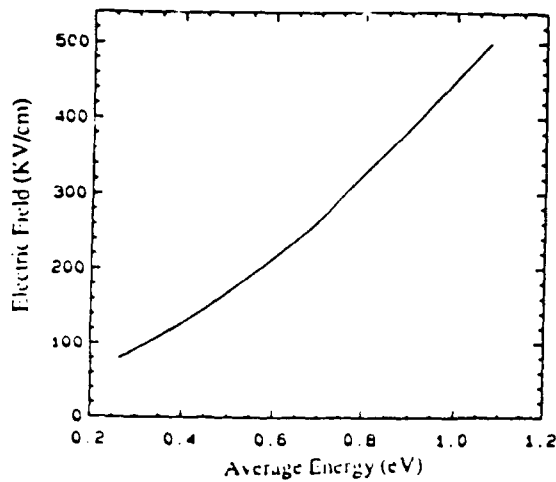


Figure 1 Average energy vs. electric field generated by homogeneous field Monte Carlo for use in determining the effective electric field profile.

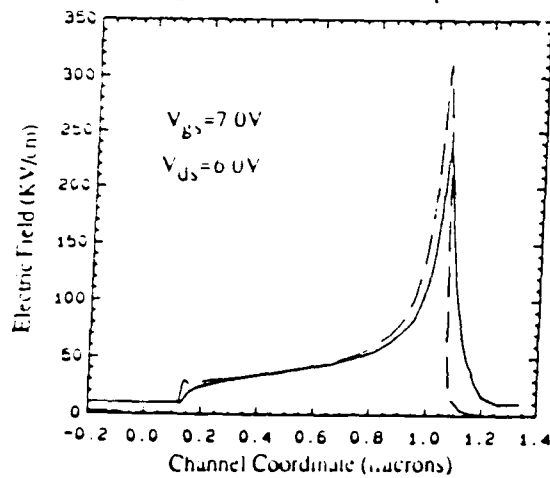


Figure 2 The effective electric field in the channel, parallel to the interface, is compared with the actual electric field.  $L/\lambda = 1.2 \mu\text{m} / 50 \mu\text{m}$ ,  $t_{\text{ox}} = 150 \text{\AA}$ .

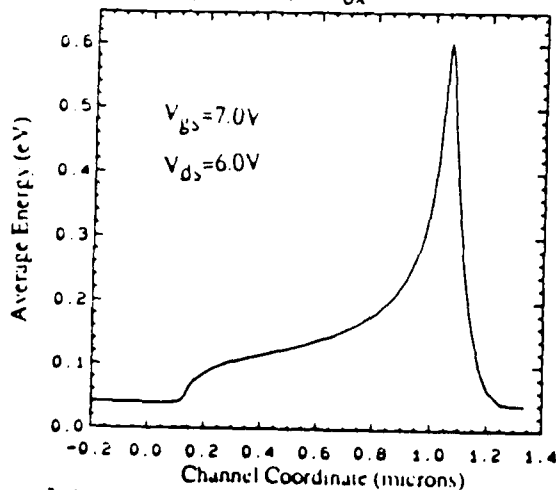


Figure 3 Average energy vs. position along the channel. Gate oxide begins at  $x=0$ .

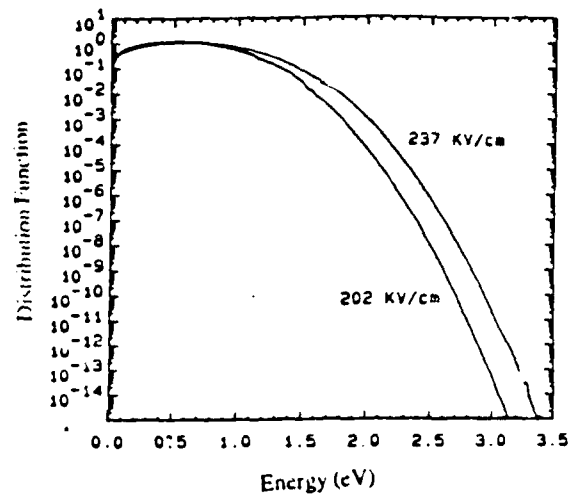


Figure 4 Distribution functions, calculated using ET-MC method, at channel coordinates  $1.045 \mu\text{m}$  and  $1.061 \mu\text{m}$  which correspond to effective field values of  $202 \text{ KV/cm}$  and  $237 \text{ KV/cm}$  respectively.

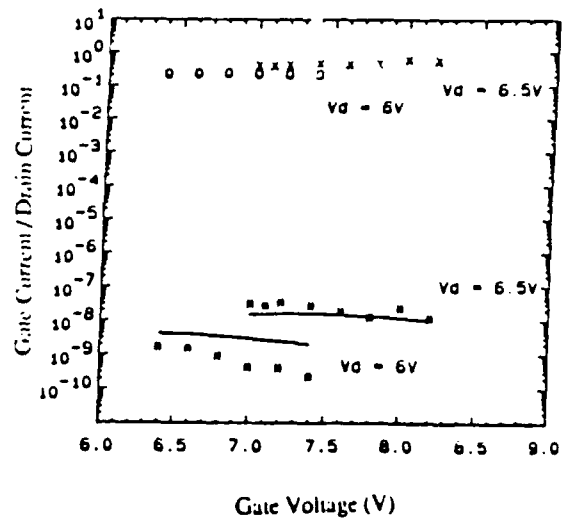


Figure 5 Values calculated for gate current using the presented ET-MC method and Richardson's equation are compared with experiment. The asterisks are calculated using ET-MC method; the open circles and 'x' signs are calculated with Richardson's equation; the solid lines are experimental values.